Preliminary studies for model-based system inversion of a 80 m tall guyed mast under dynamic wind loads

B. Clavelo [1,2], **P. Martín** [2], **K. Maes** [1], **V. Elena** [2], **G. Lombaert** [1]
[1] KU Leuven, Department of Civil Engineering,
Kasteelpark Arenberg 40, B-2448, Leuven, Belgium
email: **brunojorge.claveloelena@kuleuven.be**

[2] CUJAE, Department of Structures
114th St. 11901, Havana, Cuba

Abstract

Several guyed masts telecommunication towers have collapsed in the last decades due to dynamic wind loads, evidencing the need to improve the computational and load models used in their design. Model-based system inversion techniques are a powerful tool to estimate the loads acting on a structure using a reduced set of measured responses and a model representing the dynamic behavior of the structure. These techniques have not been implemented yet for tall guyed masts with non-linear behavior. This work describes the preliminary studies conducted to implement a model-based system inversion for an operating 80 m tall mast in Cuba. The applicability range of a state-of-the-art modal load reconstruction method, which assumes linear structural behavior, is investigated based on synthetic measurement data for different wind velocities. It is found that the reconstruction of the modal loads is successful for low wind velocities. For higher wind velocities, it is investigated how the non-linear behavior of the mast affects the proposed system inversion method.

1 Introduction

Guyed telecommunication towers play a primary role in the development of modern society. These structures are highly sensitive to dynamic wind loads due to their slenderness, low weight and non-linear behavior, introduced by the presence of prestressed cables to provide the lateral stiffness to the mast. In recent years, Cuba has suffered the passage of numerous hurricanes, tropical storms and other large-scale meteorological phenomena, causing the total or partial collapse of several telecommunications towers of which approximately 80% are guyed masts [1]. These failures evidence the uncertainties still existent in their design process. A relevant problem in structural design of guyed masts is the correct assessment of the wind forces acting on the structures, since direct measurement of wind loads is not possible due to the lack of suitable wind force transducers and the large spatial distribution of wind force fields. Model-based system inversion techniques present an alternative solution for the estimation of the system inputs, using only a set of measured responses and a dynamic model of the structure.

Several methods have been developed to estimate wind forces from measured responses on tall buildings [2], cable-stayed bridges [3] and high-rise towers [4]. Moreover, various frequency-domain [5, 6] and time-domain [7, 8] approaches with regularization schemes have been investigated. Although several researchers [9, 10, 11] have conducted studies to assess the structural response of guyed masts from measured response, there are limited studies in the estimation of wind forces using system inversion techniques. Law et al. [12] identified the along-wind dynamic wind loads on 50-m-tall guyed mast using synthetic displacement responses based on a modified iteration scheme. However, the non-linearity of the response is not considered since the cables are modeled as linear truss elements with time-invariant stiffness. More recently, Amiri and Bucher [13] proposed a time-domain method for the reconstruction of modal wind loads on a small-scale guyed mast in Austria, based on modal impulse response matrices obtained from experimentally

identified modal parameters and assuming a linear behavior. This method is further discussed in section 4. To the author's best knowledge, there are no studies focusing on the system inversion of tall guyed masts, considering the influence of the non-linear behavior in the estimated wind forces.

In this work, preliminary studies are conducted to implement the system inversion of a fully operating 80-m-tall guyed mast, located in the region of Santa Cruz del Norte, Cuba. The study is based on simulations obtained from a detailed finite element model of the structure that is developed in SAP2000. First, the influence of the non-linearity in the structural response is investigated through a non-linear dynamic analysis in the time-domain, using synthetic wind load functions generated for different wind velocities. Secondly, the applicability range of a state-of-the-art frequency-domain modal load reconstruction method, which assumes linear structural behavior, is investigated based on synthetic measurement data for different wind velocities. It is found that the reconstruction of the modal loads is successful for low wind velocities. For higher wind velocities, it is investigated how the non-linear behavior of the mast affects the proposed system inversion.

2 Model description and sensor layout

2.1 Description of the structural model

The structure selected for the study is a guyed mast telecommunication tower located in the region of Santa Cruz del Norte, Mayabeque, Cuba. The selected tower is composed of a 75.5-m-high shaft, with a 4.5-m-high tubular mast located at the top, for a total height of 80 m. The lateral stiffness of the structure is guaranteed by means of 21 cables distributed in 3 directions, spaced at $120°$ in plan. Each direction has 7 cables distributed in 5 levels, at a rate of one cable per level, with the exception of levels 2 and 4, which present two cables due to the presence of anti-torsional devices. The geometric characteristics of the tower and the cables are detailed in Figure 1.

All the elements of the shaft are L-shaped steel sections of equal sides and structural steel ASTM A-36. The columns are conformed by back-to-back $L750 \times 80$ mm sections, forming an interior angle of $60°$. The shaft is braced by means of horizontal braces spaced every one meter and crossed diagonals on each face, formed in both cases by $L500 \times 50$ mm sections. The cross section of the shaft is stiffened by internal braces, formed by $L400 \times 40$ mm steel sections, as shown in Figure 1. In the case of the cables, the first four levels consist of $1 \times 7 + 0$ braided steel cables with a diameter $\phi = 13$ mm (breaking load $P_u = 162$ kN), while the last level of cables consists of $1 \times 19 + 0$ braided steel cables with diameter $\phi = 16$ mm (breaking load $P_u = 235$ kN). High elastic limit structural steel is used in all cables. The properties of the materials are shown in Table 1 and are considered time-invariant for the study.

A finite element model is created using the commercial software SAP2000 (version 21). The shaft and the mast are modeled in detail as a three-dimensional lattice structure and the cables as special prestressed "cable" type elements, taking into account the structural characteristics of each element. The connections between the shaft elements are considered as hinges in all cases except for the columns and the mast located at the top. In the first case, the columns are modeled continuously from the base to the top of the shaft because the connection between them is made by means of rigid plates, bolted on both legs of the connected L-sections, thus ensuring the transmission of bending moments. For the case of the tubular mast, it is considered continuous because it is made up of a 6-m-long continuous solid steel tube. The supports at the base of the columns are considered as fixed, restricting the 6 degrees of freedom (DOFs) in space, while the connection of the cables to the shaft and the ground is considered as a hinge in both cases, due to the inability of the cables to absorb bending moments. A similar finite element model is created in the MATLAB toolbox Stabil [14], to obtain the structural response for a linear analysis. For this model, the cables are modeled as linear truss elements. Hence, in order to account for the effect of the initial cable pretension, the modified stiffness and mass matrices used in the analysis are extracted from SAP2000.
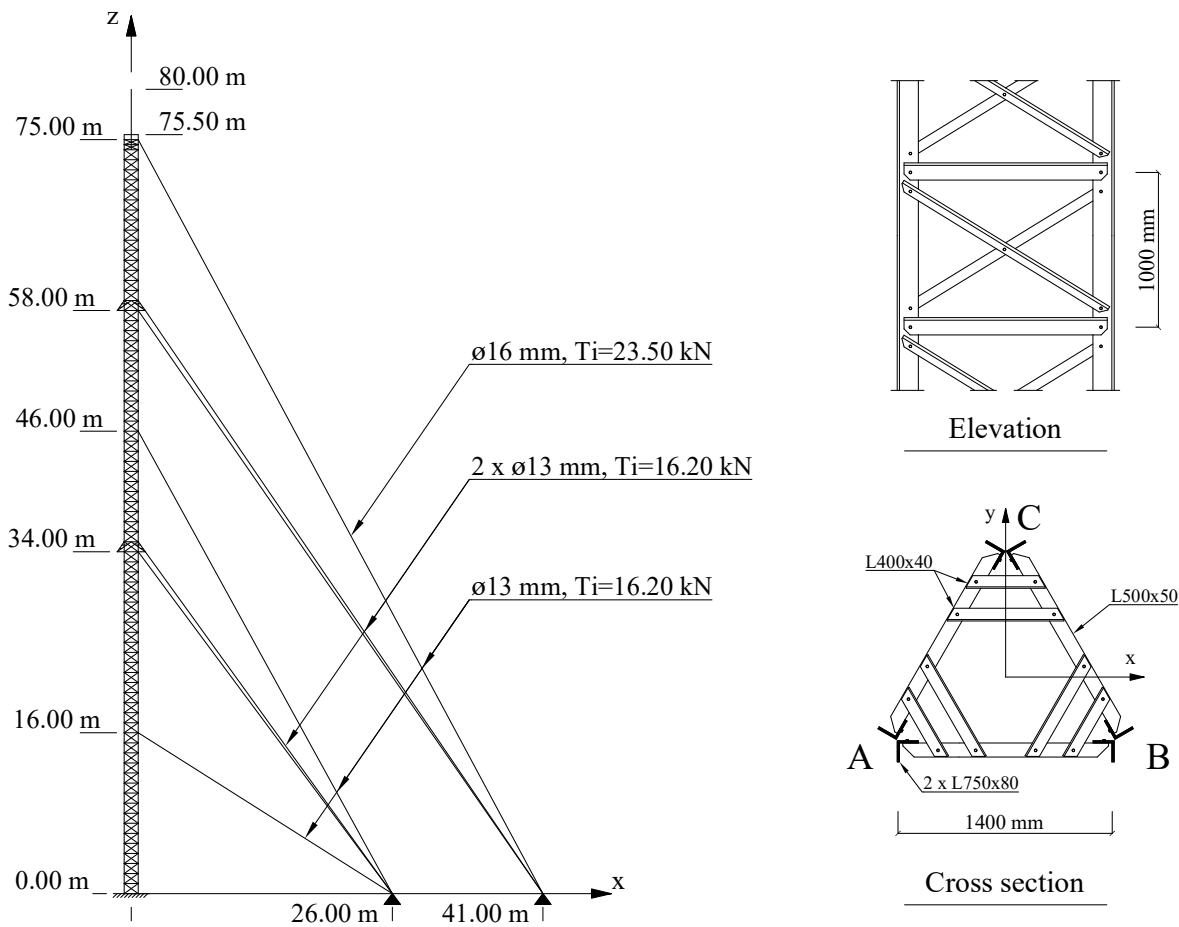
Figure 1: Geometry of the tower.

Table 1: Properties of structural steel.

Parameter	Shaft elements	Cables
Weight per unit volume [ρ]	76.97 kg/m^3	76.97 kg/m^3
Young's modulus [E]	1.999×10^8	1.999×10^8
Poisson coefficient [ν]	0.3	0.3
Coefficient of thermal expansion [α]	1.17×10^{-5}	1.17×10^{-5}
Yield Stress [f_y]	250 MPa	1600 MPa
Ultimate Stress [f_u]	400 MPa	2000 MPa

2.2 Loads

The loads considered in the analysis are: a) the self-weight of the elements, b) the prestressing load on the cables, c) the weight of the antennas and electrical panels on the structure and d) the loads due to wind action on the structure. The self-weight of other auxiliary elements, such as stairs and support grids, are not considered in the finite element model. The masses of the antennas are assigned to the finite element model at the nodes where the columns and the braces intersect, with the aim of simplifying the analysis of the structure. The antenna masses present on the tower are listed in Table 2.

The pretension load on the cables is considered as a target force applied at the end of the cable connected to the ground. The target force load is a special type of loading where a deformation load is iteratively applied to the cable in the specified point until the desired cable tension is achieved. The target tension for each cable, T_i, is selected as 10% of the rupture load of the cable, which is in the range of values specified by design codes [15]. The specified value of target tension for each cable is shown in Figure 1.

Table 2: Distribution of antenna masses on the tower

Antenna type	Span	Heigth (m)	Weight (kg)	Vertex	Area (m^2)
Dish	6	17	9	A	1.54
Dish	6	18	5.5	B	1.13
FM Antenna	8-9	$23.5 - 26.5$	6	B-C	-
Electrical box	11	$31 - 32.5$	38.7	A, B, C	0.72
Closed dipole antenna MOVITEL (4)	12-14	$36.5 - 41$	5	A	-
Open dipole antenna FM (4)	16-19	$46 - 55$	4.5	A	-
UHF antennas (2)	20-21	60, 61	13.61	A, C	2.9
Band III antenna, Dipole (2)	22	$63.5 - 66.5$	25	A,B,C,D	0.6
Band III antenna, Dipole (4)	24	$69.5 - 72.5$	340 (Total)	A-B, B-C	1.89
UHF antennas	Mast		15.65	6 x 4	2.9

The action of the wind on the structure is simulated by means of time-varying synthetic wind loads, generated via the procedure proposed by Fernández [16], which has been successfully applied in previous research on telecommunication towers in Cuba. This procedure is based on the generation of synthetic wind velocity records, for which the corresponding wind load records are then obtained. Those are applied to the finite element model in SAP2000. For the present work, only loads acting in the global y- direction are considered.

For the generation of the synthetic wind records, the following considerations are taken into account: a) the turbulence is treated as a time-dependent stationary random stochastic process, with zero mean and Gaussian behavior; b) the wind field is discretized into 12 points spaced every 6 meters along the height of the mast, that represent the force locations; c) the wind velocity records at each point are generated for a total time T = 655 s, with a time step $\Delta t = 0.005$ s corresponding to a sampling frequency of 200 Hz, for a total of N = 2^{17} steps; d) a simplified model for turbulence is assumed generating only the longitudinal component, u_y in the y- direction; e) the spatial coherence function was obtained according to the equation proposed in [17], with an exponential decay coefficient $k_z = 10$ and f) the generation method adopted is the spectral representation via Cholesky decomposition. The decomposition of the cross-power spectrum matrix XPSD is performed using the formulations proposed by Veers [18].

The vertical profile of the mean wind velocity, $\bar{u}(z)$, is calculated with the potential law, according to equation (1),

$$\bar{u}(z) = \bar{U}_0 \left(1.7 \left(\frac{z}{z_g} \right)^\alpha \right) \tag{1}$$

where $\bar{U}_0$ is the basic wind velocity at a reference height of 10 m, in m/s; z is the generation height in m; $z_g = 250$ m is the gradient height for the terrain type and $\alpha = 0.10$ is an exposure coefficient depending on the terrain type.

The variation of the energy content of the turbulent wind functions is described using Von Kármán spectral equation (2),

$$S(\omega) = \frac{4\sigma_u^2 \, fL_u/h}{\omega[1 + 70.8(fL_u/h)^2]^{5/6}} \tag{2}$$

where ω is the angular frequency in rad/s; h is the reference height in m; L_u is the integral scale of the longitudinal component of turbulence; $f = \omega z/\bar{u}(z)$ is the Monin coordinate; and σ_u^2 is the variance of the longitudinal component of the turbulence, obtained according to the model described by Solari and Piccardo in [19],

$$\sigma_u^2 = [6 - 1.1\ \mathrm{arctg}(\ln(z_0) + 1.75)] * u_*^2 \tag{3}$$

where u_* is the shear velocity obtained at a reference height of $h = 10$ m and $z_0 = 0.05$ m is the roughness length for the terrain type.

Using the previously described procedure, eight sets of turbulent wind velocity records are generated for different basic wind velocities $\bar{U}_0$, ranging from 2 m/s (still-air conditions) to 30 m/s (category 4 hurricane), in intervals of 4 m/s, in order to study the effects on non-linearity in the response of the structure and the system inversion. The initial 55 s of each generation are discarded. This reduces the total duration of the signal to 600 s. The results of the simulation are exemplified in Figure 2, where the power spectrum and a wind velocity time history are shown for a basic wind velocity $\bar{U}_0 = 6$ m/s
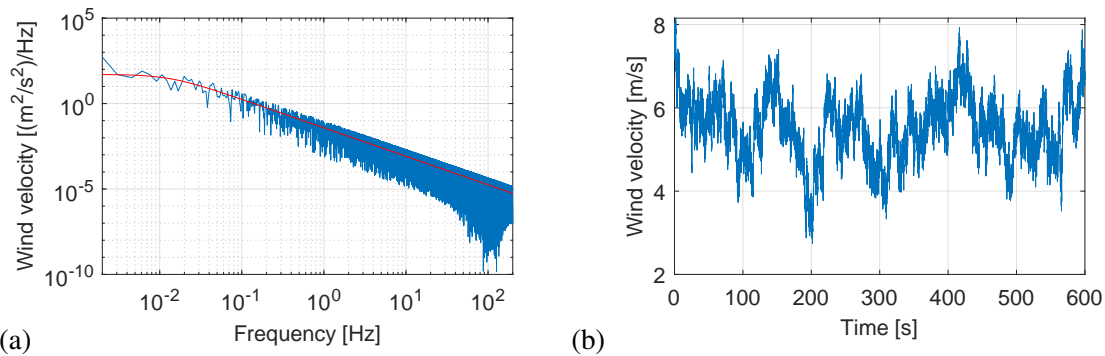

Figure 2: (a) Power spectrum and (b) corresponding time history of the generated wind velocity at a single point for $\bar{U}_0 = 6$ m/s.

The wind load records are obtained by means of equation (4),

$$P(t) = \frac{1}{2}\rho\,(u(t))^2\,A_{\mathrm{ref}}C_{\mathrm{f}} \tag{4}$$

where $P(t)$ is the instant value of the wind load in kN; $\rho = 1.184$ kg/m^3, is the air density at an average temperature of 25°C; $u(t)$ is the instant value of the wind velocity in m/s; A_{ref} is the average tributary area of the shaft corresponding to the generation height in m^2 and C_{f} is the force coefficient.
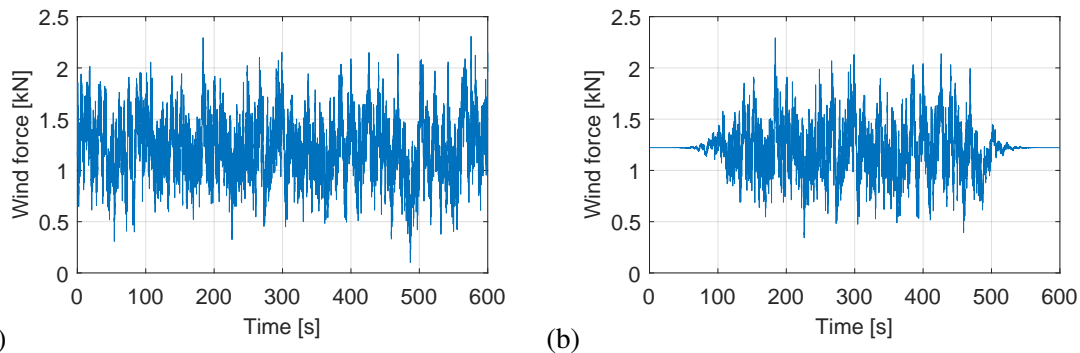

Figure 3: (a) Original time history and (b) treated time history of the generated wind load function at a single point for $\bar{U}_0 = 22$ m/s.

The wind load records are processed to obtain the final wind loads in a three-step process: 1) each wind load record is de-trended by substracting the mean value and a 5th order Butterworth time window is applied to

reduce the leakage by forcing the amplitude of the de-trended signal to zero at each end of the window; 2) the mean value is added back to the windowed signal, ensuring the periodicity of the wind load record around the mean value; 3) the signal is decimated by a factor of 2 with a two-way, low-pass, 9th order Chebysev filter with a cut-off frequency of 40 Hz. The original and treated wind load records are compared in Figure 3.

2.3 Description of the modal parameters

This section presents the modal parameters obtained from the SAP2000 model for the initial equilibrium state of the mast under its own weight, the weight of the antennas and the initial tension of the cables.

Table 3 shows the natural frequencies of the first 12 global modes shapes of the structure. These modes include the first 5 global bending modes in each of the main bending directions (x-, y-), and the first two torsional modes with respect to the vertical axis (z-). In the studied structure, paired modes are observed with respect to the main bending directions x- and y-, with similar mode shapes and natural frequencies, in correspondence with the symmetry of the cross section and the distribution of the guys, as well as the quasi-symmetric distribution of the mass. For this reason, the global mode shapes are presented in Figure 4 only for the global bending direction y- and the torsion around the vertical axis z-.
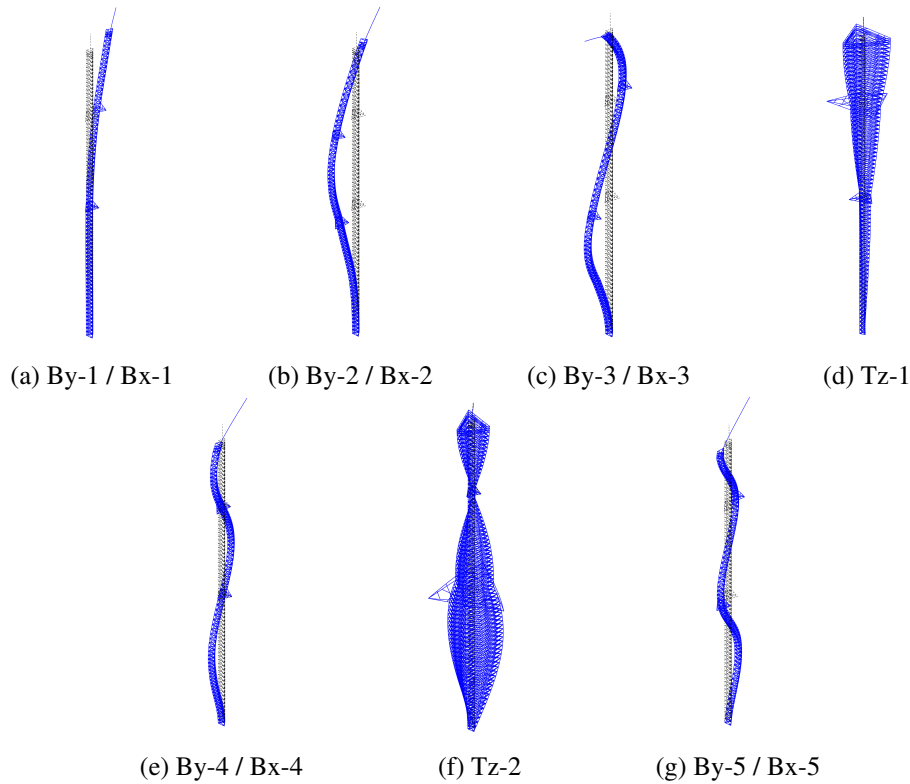

(a) By-1 / Bx-1   (b) By-2 / Bx-2   (c) By-3 / Bx-3   (d) Tz-1

(e) By-4 / Bx-4   (f) Tz-2   (g) By-5 / Bx-5

Figure 4: Global mode shapes.

Table 3: Natural vibration frequencies.

Mode	1	2	3	4	5	6	7	8	9	10	11	12
Type	By-1	Bx-1	By-2	Bx-2	By-3	Bx-3	Tz-1	By-4	Bx-4	Tz-2	By-5	Bx-5
Frequency [Hz]	1.521	1.521	2.612	2.614	3.762	3.766	4.228	5.623	5.630	7.269	7.586	7.594

By: Bending mode in y- axis; Bx: Bending mode in x- axis; Tz: Torsional mode around z- axis

2.4 Sensor layout

Figure 5 shows the sensor layout adopted in the system inversion. The simulated response consists of 16 displacements in y- direction and 8 displacements in the x- direction. The measurement levels are evenly distributed along the height of the structure. For every level, three DOFs are selected, in a configuration which enables capturing both bending and torsion of the mast. The sensor labels are composed as follows: D$\alpha - \beta\gamma$; where α indicates the level of the sensor in height, β the vertex where the sensor is placed and γ the measured direction.

Whithin the frame of this feasibility study, a displacement-based system inversion is assumed. The authors realize, however, that a practical application would rely on acceleration rather than displacement data. The results of the study, however, could be readily extended to the case of acceleration measurements.
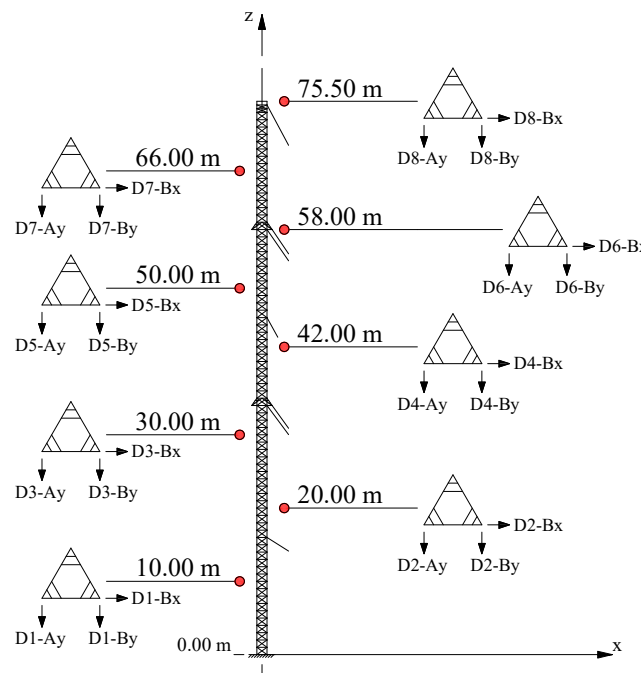

Figure 5: Sensor layout adopted for the system inversion.

3   Influence of non-linearity in response estimation

The response of guyed mast telecommunication towers to dynamic wind loading is influenced by the non-linear behavior of the structure. This non-linearity arises from the large displacements of the shaft under horizontal loads, which modify the tension in the cables, leading to a change in their individual catenary, their stiffness and subsequently, the overall stiffness of the structure [20]. A study conducted for different models of guyed masts in Cuba [21], shows that for basic wind velocities up to 20 m/s, the maximal displacements of the tower obtained through a quasi-static analysis can be estimated with an error $\epsilon < 5\%$, using a linear approximation. However, the effect of the non-linearity in the estimation of the dynamic response is not investigated. In this study, the influence of the non-linear behavior on the structural (dynamic) displacements is investigated for different wind velocities. This involves the comparison of the results obtained for two different analyses.

In the first analysis, the structural response to the dynamic wind loads generated in section 2.2 is obtained through a non-linear time history analysis conducted in software SAP2000. First, the initial stiffness matrix used in the analysis is the modified stiffness matrix obtained for the equilibrium position under the effect of self-weight, antenna masses and cable pretension.Next, for every step n of the analysis, the stiffness matrix of the system is updated based on the deformation of the structure and the corresponding variation of cable

tensions. The updated stiffness is used as the initial stiffness at the beginning of time step $n+1$. This analysis accounts for the effect of cable pretension in the modification of the global stiffness matrix and the non-linear response of the structure. The solution is found by means of a direct integration scheme considering P-Delta and large displacements effects. The unconditionally stable Newmark-Beta method ($\gamma = 0.5$, $\beta = 0.25$) is used for the numerical solution of the system and a Rayleigh proportional damping matrix is assumed with damping ratios $\xi = 0.005$ for modes 1 and 2. The damping ratios are estimated from wind tunnel studies for guyed masts under different wind load conditions [22].

In the second analysis, the linear response to the wind loads is obtained by means of modal superposition in the frequency domain. The modal characteristics assumed in the linear calculation are those obtained from the modified stiffness and mass matrices extracted from SAP2000 which account for the effect of the initial cable pretension. The modal decomposition of the system and the solution of the modal equations are performed using the MATLAB toolbox Stabil [14].

The structural displacements at the selected degrees of freedom (see Figure 5) are compared. As an example, Figure 6 compares the displacement response at sensor D8-By for different wind velocities and considering both the non-linear and the linear response.
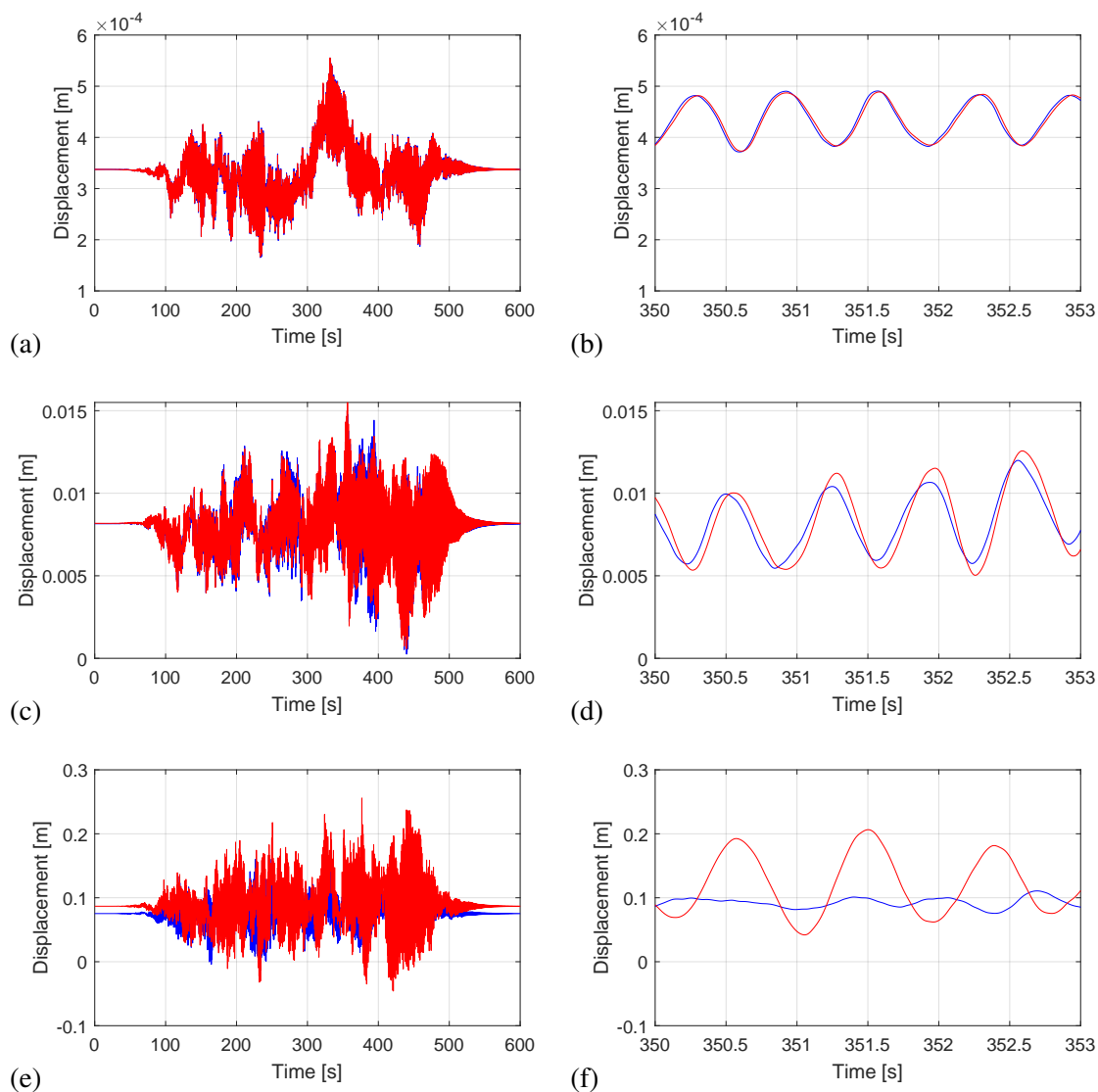

Figure 6: Displacement response (left) obtained at DOF corresponding to sensor D8-By for linear analysis (blue) and non-linear analysis (red), and detailed time history (right) of a three second interval, for different basic wind velocities: 2 m/s (a,b), 10 m/s (c,d) and 30 m/s (e,f).

It can be observed that the consideration of the non-linearity does not generate large discrepancies for low wind velocities (see Figure 6a). As the wind velocity increases, however, (Figures 6c and 6d) the response time history shows larger deviations in the magnitude of the displacements, with larger values obtained for the non-linear analysis, as well as an elongation of the period of the non-linear response, which can be explained by the reduction of the system stiffness due to the lateral displacements of the mast. Additionally, it is noted that for higher wind velocities ($\bar{U}_0 \geq 22$ m/s) there is a visible offset in the response for the mean wind velocity. This behavior can be explained by a large decrease of the tension in the leeward cables due to the horizontal displacement of the shaft, causing a large reduction of the overall stiffness. For the remaining DOFs a similar behavior is observed.

In order to quantify the relative error ϵ between the linear and the non-linear response, the Root Mean Square Relative Error (RMSRE) is calculated for all the compared DOFs and for all basic wind velocities considered, following equation (5),

$$\epsilon = \sqrt{\frac{\sum_{l=1}^{N} \left(u_l^{\mathrm{L}} - u_l^{\mathrm{NL}} \right)^2}{\sum_{l=1}^{N} \left(u_l^{\mathrm{NL}} \right)^2}} \tag{5}$$

where N is the total number of time steps; and u_l^{L} and u_l^{NL} are the displacements obtained by linear modal superposition and non-linear time history analysis in SAP2000, respectively, for each time step l.

The relative errors (RMSRE) in the estimation of the response for the basic wind velocities considered in the study are shown in Figure 7 for three responses located at different heights of the mast (10 m, 42 m and 75.5 m). It is evidenced that disregarding the effect of the non-linearity for basic wind velocities over 10 m/s, leads to errors in the estimation of the dynamic response in the range of 10 to 44%.
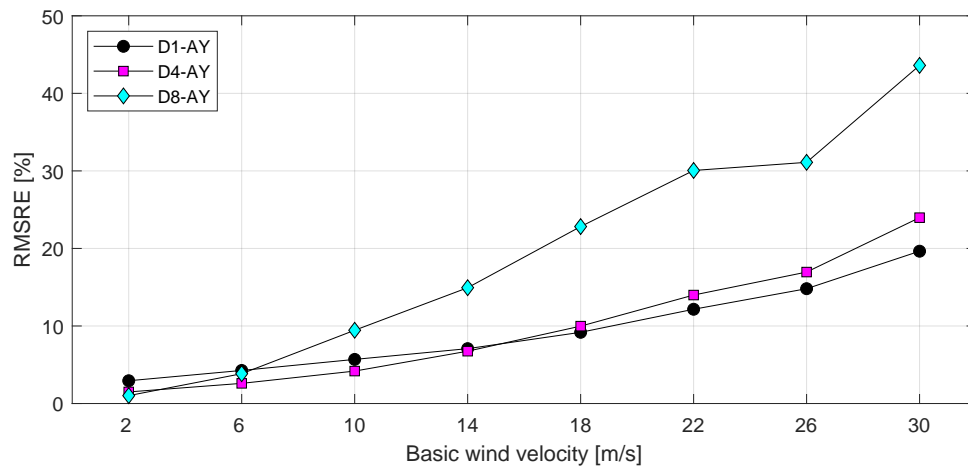

Figure 7: Root Mean Square Error obtained for different wind velocities at three DOFs.

4 Influence of non-linearity in system inversion

The method proposed by Amiri and Bucher [13] allows the reconstruction of the acting modal wind loads from a set of response measurements on the structure. This procedure is based on the decomposition of the measured responses in their modal components by means of the pseudo-inverse of the incomplete mode shapes matrix. The Modal Impulse Response Matrices of the system are then generated from experimentally identified modal parameters and used to establish the input-output relationship between the modal responses and modal loads. For the present work, an equivalent procedure is implemented in the frequency-domain, using the modal parameters obtained from the FEM for the first 12 modes of the structure and the non-linear displacement response $\mathbf{u}_{\mathrm{d}}$ at the 24 proposed sensor locations (see Figure 5).

The steps of the procedure implemented in the frequency-domain are the following:

1. The Fourier transform of the displacement time histories, denoted as $\mathbf{u}_\mathrm{d}(\omega)$, is computed by means of the discrete Fourier transformation.

2. For every frequency ω, the displacement response is decomposed in the modal components as follows,

$$\hat{\mathbf{x}}(\omega) = [\mathbf{S}_\mathrm{d}\boldsymbol{\Phi}]^\dagger\,\mathbf{u}_\mathrm{d}(\omega) \tag{6}$$

where $\hat{\mathbf{x}}(\omega) \in \mathbb{R}^{n_\mathrm{m}\times 1}$ is the vector of estimated modal coordinates; $\mathbf{S}_\mathrm{d} \in \mathbb{R}^{n_\mathrm{d}\times n_\mathrm{dof}}$ is a spatial selection matrix specifying the output locations, where the number of modes n_m and the number of outputs n_d equal 12 and 24, respectively, and n_dof is the total number of DOFs in the finite element model. $\boldsymbol{\Phi} \in \mathbb{R}^{n_\mathrm{dof}\times n_\mathrm{m}}$ is the mass-normalized mode shape matrix and $\mathbf{u}_\mathrm{d}(\omega) \in \mathbb{R}^{n_\mathrm{d}\times 1}$ is a vector containing the displacements at the sensor locations.

3. The validity of the decomposed modal coordinates is checked by means of its power spectrum. Each modal response must only have one dominant vibration frequency corresponding to the natural frequency of the system at that mode.

4. The modal transfer function matrix of the system $\mathbf{H}(\omega)$ is generated, containing the modal transfer functions for each mode j, which are obtained as follows,

$$H_j(\omega) = \frac{1}{-\omega^2 + 2\xi_j\omega_j i\omega + \omega_j^2} \tag{7}$$

where i is the imaginary unit ($i^2 = -1$), $\omega \in \mathbb{R}$ is the angular frequency in rad/s, and $\omega_j \in \mathbb{R}$ and $\xi_j \in \mathbb{R}$ are the natural frequency and modal damping ratio of mode j, respectively.

5. The modal wind loads are estimated from the modal transfer function matrix $\mathbf{H}(\omega)$ and the estimated modal coordinates $\hat{\mathbf{x}}(\omega)$ in a least-squares sense:

$$\hat{\mathbf{p}}(\omega) = \mathbf{H}(\omega)^\dagger\hat{\mathbf{x}}(\omega) \tag{8}$$

6. The time history of the estimated modal loads is obtained by means of the inverse discrete Fourier transform.

The applicability range of this procedure for the estimation of the modal loads is assessed for 8 different values of basic wind velocity from 2 m/s to 30 m/s in intervals of 4 m/s. For every set of loads corresponding to a basic wind velocity, the non-linear structural displacements are obtained at the 24 DOFs corresponding to the proposed sensor locations, generating the reduced response matrix $\mathbf{u}_\mathrm{d}$. Equations (6) to (8) are then used to obtain the estimated modal loads $\hat{p}_j$.

The estimated modal loads $\hat{p}_j$ are compared in the time-domain to the actual modal loads p_j, which are obtained as follows,

$$p_j(t) = \boldsymbol{\varphi}_j^\mathrm{T}\mathbf{S}_\mathrm{p}\mathbf{p}(t) \tag{9}$$

where $\mathbf{S}_\mathrm{p} \in \mathbb{R}^{n_\mathrm{dof}\times n_\mathrm{p}}$ is a spatial selection matrix specifying the input locations, with n_p the number of inputs ($n_\mathrm{p} = 12$), $\boldsymbol{\varphi}_j \in \mathbb{R}^{n_\mathrm{dof}\times 1}$ is the mass-normalized mode shape vector for mode j, and $\mathbf{p}(t) \in \mathbb{R}^{n_\mathrm{p}\times 1}$ is the force time history vector.

Figure 8 compares the actual and estimated modal loads for modes 1 and 12, for three different magnitudes of excitation, i.e. three sets of wind loads for different basic wind velocities. It is observed that for the low wind velocities (Figure 8a and 8b), the modal loads can be accurately estimated for the low-order modes. For the higher-order modes, the dynamic component of the estimated and actual modal wind loads is very

similar, but a large offset is observed between the mean values. As the wind velocities increases, this offset tends to increase for all modes, as can be observed in Figures 8e and 8f. The error in the mean value of the modal wind loads is expected to be attributed to the contribution of the out-of-band modes which have not been accounted for in the system inversion. These discrepancies are the subject of ongoing investigation.
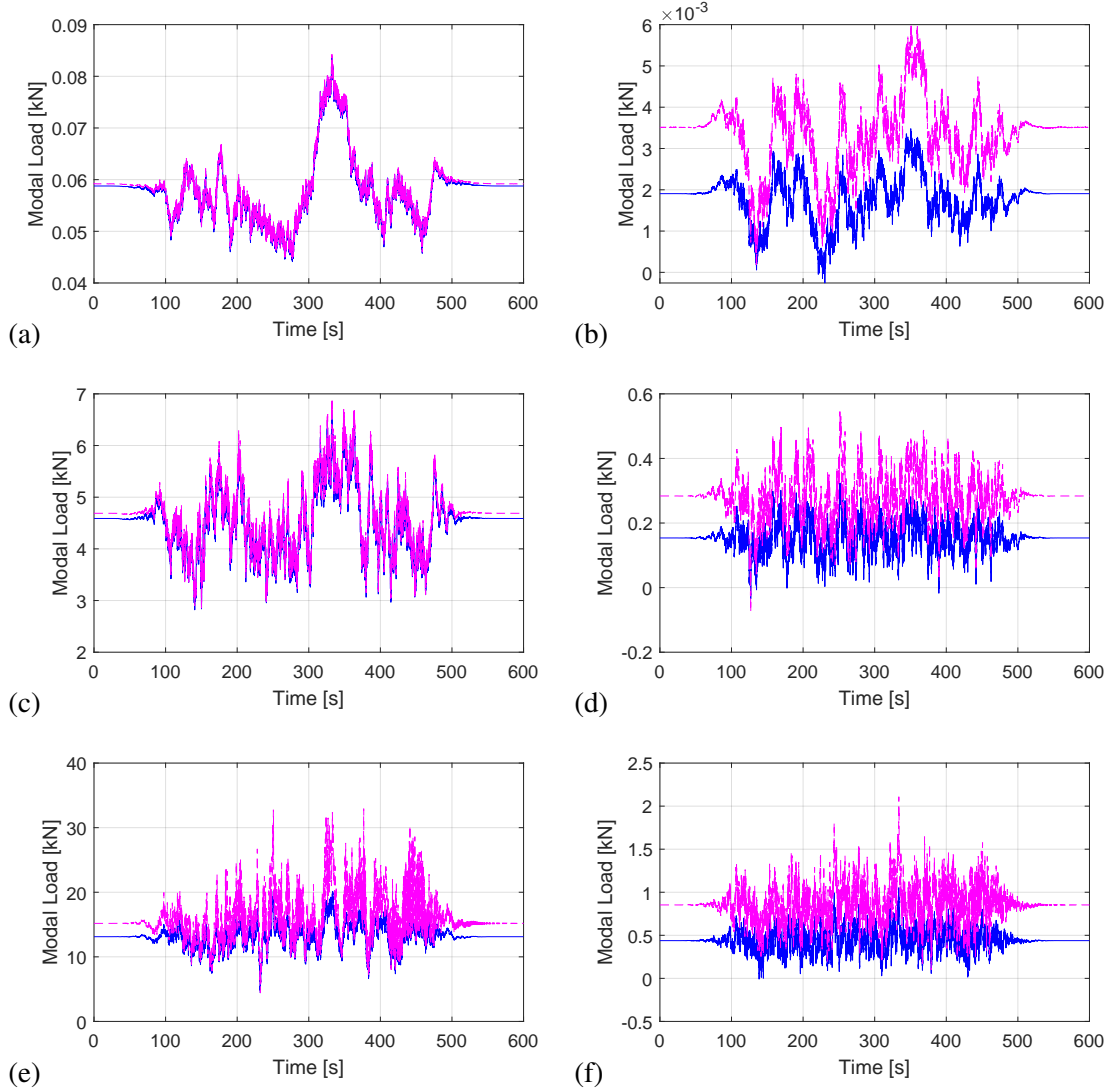

Figure 8: Comparison of decomposed modal loads, p_j (blue) and estimated modal loads $\hat{p}_j$ (magenta) of modes 1 (left) and 12 (right), for different basic wind velocities: 2 m/s (a,b), 18 m/s (c,d) and 30 m/s (e,f).

Similar to the comparison in section 3, the relative error between the actual and the estimated modal wind loads is quantified by means of the Root Mean Squared Relative Error:

$$\epsilon = \sqrt{\frac{\sum_{l=1}^{N} \left(\hat{p}_{j_l} - p_{j_l}\right)^2}{\sum_{l=1}^{N} \left(p_{j_l}\right)^2}} \tag{10}$$

Table 4 shows the RMSRE for each of the 12 modes j considered in the system inversion and for each value of basic wind velocity $\bar{U}_0$. For the first seven modes of the structure, the modal loads can be estimated with a relative error under 10% for basic wind velocities up to 22 m/s. For modes 8 to 12, the error in the estimation is higher ($\epsilon > 23\%$), independently of the magnitude of the excitation and shows small variations in relation to the basic wind velocities up to 26 m/s. This could be explained by the relatively large error in the mean wind load, as discussed previously.

Table 4: RMSRE obtained in the estimation of the modal loads $\hat{p}_j$ for different basic wind velocities.

$\bar{U}_0$ (m/s)	RMSRE (%)											
	By-1	Bx-1	By-2	Bx-2	By-3	Bx-3	Tz-1	By-4	Bx-4	Tz-2	By-5	Bx-5
2	0.87	0.94	0.75	0.33	7.72	5.23	8.63	24.38	32.27	128.28	87.06	86.78
6	1.16	0.98	0.78	0.42	7.54	5.30	9.21	23.65	30.33	123.94	78.74	78.72
10	1.41	0.92	0.69	0.38	7.54	5.30	9.27	24.02	30.74	128.18	81.91	81.86
14	1.82	0.94	0.54	0.47	7.61	5.34	8.65	23.97	30.72	127.79	82.26	82.25
18	2.68	1.50	0.59	0.90	7.47	5.26	7.84	23.97	30.83	129.14	83.78	83.79
22	5.14	3.93	1.76	2.19	7.43	5.32	6.45	23.83	30.80	132.36	85.72	85.83
26	10.11	8.84	5.30	5.78	8.25	6.43	5.61	23.72	30.95	139.06	88.96	89.24
30	30.60	29.23	19.49	20.12	19.46	17.91	19.49	26.64	34.93	167.38	99.30	100.09

For the majority of the modes, the error in the estimated modal wind velocities does not vary significantly when the basic wind velocities changes from 2 to 18 m/s. However, for basic wind velocities above 18 m/s, the error in the estimation increases significantly with the wind velocity. As such, it can concluded that the non-linearity in the structural behavior for the considered case cannot be disregarded when performing system inversion for wind speeds above 18 m/s.

5   Conclusions

Although linear methods significantly reduce the computational effort in the response estimation and inversion of a system, they can lead to large errors in the estimation of the dynamic response of guyed masts under lateral wind load. Results show that the dynamic response of the guyed mast studied can be accurately estimated using a linear analysis for basic wind velocities up to 10 m/s. For higher wind velocities, a non-linear analysis results in response predictions which are up to 45% larger. The validity of a frequency-domain method for the inversion of guyed masts is investigated for increasing wind velocity. It is found that the modal loads for the low-order modes can be estimated with an error under 10% for basic wind velocities up to 22 m/s. For higher basic wind velocities, the error in the estimation of the modal loads increases significantly, with values up to 30% for the first 7 modes. The estimation of the modal loads for higher-order modes leads to large errors independently of the basic wind velocity. These are most likely explained by the influence of the out-of-band modes, which have not been accounted for in the system inversion.

References

[1] V. Elena Parnás, I. Fernández Lorenzo, and P. Martín Rodríguez, "Structural failure on telecommunication guyed mast under extreme winds." 14th International Conference on Wind Engineering, Porto Alegre, Brasil, 06 2015.

[2] I. Nagashima, R. Maseki, Y. Asami, J. Hirai, and H. Abiru, "Performance of hybrid mass damper system applied to a 36-storey high-rise building," *Earthquake Engineering & Structural Dynamics*, vol. 30, no. 11, pp. 1615–1637, Nov. 2001.

[3] K. Maes, S. Gillijns, and G. Lombaert, "A smoothing algorithm for joint input-state estimation in structural dynamics," *Mechanical Systems and Signal Processing*, vol. 98, pp. 292–309, Jan. 2018.

[4] L. Zhi, Q. Li, and M. Fang, "Identification of Wind Loads and Estimation of Structural Responses of Super-Tall Buildings by an Inverse Method: Identification of wind loads and structural responses for super-tall buildings," *Computer-Aided Civil and Infrastructure Engineering*, vol. 31, no. 12, pp. 966–982, Dec. 2016.

[5] Y. Liu and W. S. Shepard, "Dynamic force identification based on enhanced least squares and total least-squares schemes in the frequency domain," *Journal of Sound and Vibration*, vol. 282, no. 1, pp. 37–60, Apr. 2005.

[6] A. Rezayat, V. Nassiri, B. De Pauw, J. Ertveldt, S. Vanlanduit, and P. Guillaume, "Identification of dynamic forces using group-sparsity in frequency domain," *Mechanical Systems and Signal Processing*, vol. 70-71, pp. 756–768, Mar. 2016.

[7] K. Li, J. Liu, X. Han, X. Sun, and C. Jiang, "A novel approach for distributed dynamic load reconstruction by space–time domain decoupling," *Journal of Sound and Vibration*, vol. 348, pp. 137–148, Jul. 2015.

[8] D. Bernal and A. Ussia, "Sequential deconvolution input reconstruction," *Mechanical Systems and Signal Processing*, vol. 50-51, pp. 41–55, Jan. 2015.

[9] P. Harikrishna, A. Annadurai, S. Gomathinayagam, and N. Lakshmanan, "Full scale measurements of the structural response of a 50 m guyed mast under wind loading," *Engineering Structures*, vol. 25, no. 7, pp. 859–867, Jun. 2003.

[10] G. Saudi, "Structural assessment of a guyed mast through measurement of natural frequencies," *Engineering structures*, vol. 59, pp. 104–112, 2014.

[11] A. Ismail, "Seismic assessment of guyed towers: A case study combining field measurements and pushover analysis," *HBRC journal*, vol. 12, no. 1, pp. 47–53, 2016.

[12] S. Law, J. Bu, and X. Zhu, "Time-varying wind load identification from structural responses," *Engineering Structures*, vol. 27, no. 10, pp. 1586–1598, Aug. 2005.

[13] A. K. Amiri and C. Bucher, "A procedure for in situ wind load reconstruction from structural response only based on field testing data," *Journal of wind engineering and industrial aerodynamics*, vol. 167, pp. 75–86, 2017.

[14] S. François, M. Schevenels, D. Dooms, M. Jansen, J. Wambacq, G. Lombaert, G. Degrande, and G. De Roeck, "Stabil: An educational Matlab toolbox for static and dynamic structural analysis," *Computer Applications in Engineering Education*, vol. 29, no. 5, pp. 1372–1389, 2021.

[15] ANSI/TIA-222-G, *Structural standards for Steel Antenna Towers and Antenna Supporting Structures*. USA: Telecommunications Industry Association (TIA), 2006.

[16] I. Fernández and V. E. Parnás, "Elements for numerical simulation of wind time series," *Revista ingeniería de construcción*, vol. 32, no. 2, pp. 85–92, 2017.

[17] M. Di Paola and I. Gullo, "Digital generation of multivariate wind field processes," *Probabilistic Engineering Mechanics*, vol. 16, no. 1, pp. 1–10, Jan. 2001.

[18] P. S. Veers, "Three-dimensional wind simulation," Sandia National Labs., Albuquerque, NM (USA), Tech. Rep., 1988.

[19] G. Solari and G. Piccardo, "Probabilistic 3-d turbulence modeling for gust buffeting of structures," *Probabilistic Engineering Mechanics*, vol. 16, no. 1, pp. 73–86, 2001.

[20] V. Elena Parnás, P. Martín Rodríguez, and A. E. Castañeda Hevia, "Structural behavior of guyed mast with asymmetrical anchors," *Journal of the Brazilian Society of Mechanical Sciences and Engineering*, vol. 35, no. 2, pp. 61–67, Jun. 2013, number: 2.

[21] V. Elena Parnás and I. Fernández Lorenzo, "No linealidad geométrica en torres atirantadas," *Revista Cubana de Ingeniería*, vol. 2, no. 3, pp. 37–44, 2011, number: 3.

[22] N. Zhu, "Wind tunnel test for guyed mast dynamic characteristics under wind loads," Ph.D. dissertation, 2007.